

Crystal Structure of SANOS, a Bacterial Nitric Oxide Synthase Oxygenase Protein from *Staphylococcus aureus*

Louise E. Bird,¹ Jingshan Ren,¹
Jiancheng Zhang,^{2,6} Neale Foxwell,²
Alastair R. Hawkins,³ Ian G. Charles,²
and David K. Stammers^{1,4,5}

¹Division of Structural Biology
The Wellcome Trust Centre for Human Genetics
Henry Wellcome Building of Genomic Medicine
University of Oxford
Roosevelt Drive
Oxford OX3 7BN
United Kingdom

²The Wolfson Institute for Biomedical Research
University College London
The Cruciform Building
Gower Street
London WC1E 6AU
United Kingdom

³School of Biochemistry and Genetics
Medical School
Catherine Cookson Building
Framlington Place
University of Newcastle-upon-Tyne
Newcastle-upon-Tyne NE2 4HH
United Kingdom

⁴Oxford Centre for Molecular Sciences
New Chemistry Building
South Parks Road
Oxford OX1 3QT
United Kingdom

Summary

Prokaryotic genes related to the oxygenase domain of mammalian nitric oxide synthases (NOSs) have recently been identified. Although they catalyze the same reaction as the eukaryotic NOS oxygenase domain, their biological function(s) are unknown. In order to explore rationally the biochemistry and evolution of the prokaryotic NOS family, we have determined the crystal structure of SANOS, from methicillin-resistant *Staphylococcus aureus* (MRSA), to 2.4 Å. Haem and S-ethylisothiourrea (SEITU) are bound at the SANOS active site, while the intersubunit site, occupied by the redox cofactor tetrahydrobiopterin (H₄B) in mammalian NOSs, has NAD⁺ bound in SANOS. In common with all bacterial NOSs, SANOS lacks the N-terminal extension responsible for stable dimerization in mammalian isoforms, but has alternative interactions to promote dimer formation.

Introduction

NO is an important signaling molecule in multicellular organisms and is generated from oxygen and arginine

by a family of nitric oxide synthase enzymes (NOS) [1, 2]. In mammals, NO regulates blood pressure, is a messenger in the peripheral and central nervous system, and also has a role as an antimicrobial and anticancer agent in host defense [1]. Three NOS isoforms have been identified, namely, neuronal (nNOS or type I), inducible (iNOS or type II), and endothelial (eNOS or type III). There is significant sequence identity between these NOS isoforms, they are homodimeric, and have two distinct catalytically active domains that may be separated by limited proteolysis [3, 4]. The N-terminal oxygenase domain contains binding sites for haem, the structural and redox cofactor tetrahydrobiopterin (H₄B), the substrate arginine linked via a calmodulin interaction site to a C-terminal reductase domain with binding sites for the prosthetic groups FMN and FAD, and the cosubstrate NADPH. In the case of nNOS there is an N-terminal extension containing a PDZ domain that interacts with proteins such as PSD-95 and syntrophin in neurons and muscle, respectively [5–7].

In recent years, structural studies of recombinant eNOS and iNOS oxygenase domains have shown that it has a novel α/β fold with an elongated shape likened to a baseball catcher's mitt [8–12]. In addition to extensive contacts across the oxygenase dimer interface there are also interactions via two regions from the N terminus (N-terminal extension). The N-terminal “hook” (two antiparallel β strands) makes both inter- and intrachain interactions, while two cysteines from a C-X₄-C motif in each subunit tetrahedrally coordinate a zinc ion to form a zinc-tetrathiolate at the dimer interface [9, 11]. In contrast, there is currently only structural information for the FAD/NADPH-containing fragment of the reductase domain of NOS, although the complete reductase domain has been modeled on the basis of its sequence homology with rat liver microsomal NADPH-P450 reductase [13, 14].

In contrast to eukaryotes, bacterial-derived NO has chiefly been regarded as an intermediate in the nitrogen cycle. In particular during dissimilatory denitrification, nitrite is reduced to NO by nitrite reductase and then further reduced to N₂O. There are two classes of nitrite reductase, namely those that contain either copper or haem as the cofactor. Neither of these enzymes is structurally or mechanistically similar to the mammalian NOSs [15]. Since the reactive nitrogen species formed from NO (e.g., peroxynitrite) are apparently toxic to bacterial cells, its level is maintained at nanomolar concentrations by tight regulation of both nitrite and NO reductases [16]. However, there is increasing evidence that bacteria can be responsive to NO levels [17, 18]. Indeed, evidence is accumulating for bacterial NOSs that are functionally homologous to eukaryotic NOSs. Biochemical studies have been carried out on enzymes from a *Nocardia* species and *Staphylococcus aureus* which indicate that they are able to convert L-arginine to

⁵ Correspondence: daves@strubi.ox.ac.uk

⁶ Present address: Department of Biological Sciences, Imperial College of Science, Technology, and Medicine, Exhibition Road, London SW7 2AZ, United Kingdom.

Key words: bacterial; NO; NOS; SANOS; *Staphylococcus aureus*; synthase

L-citrulline with concomitant evolution of NO, detected as nitrite and NO, respectively [19–22]. As NO is a pleiotropic regulator of cellular function, it has been proposed that NO generated by pathogenic organisms may have a critical pathophysiological role during infection [21]. Moreover, hypothetical proteins have been annotated in some of the sequenced bacterial genomes as being homologs of the oxygenase domain of mammalian NOSs. However, these proteins do not have an N-terminal hook, cysteines to form a zinc-tetrathiolate, or a C-terminal reductase domain [23–25]. While it is generally accepted that H₄B is not present in bacteria [23, 24], it has been suggested that genes encoding for a H₄B biosynthetic pathway are present in *Bacillus subtilis* [25]. While many of the residues that bind H₄B in mammalian NOSs are identical in bacterial NOSs, perhaps indicating a conserved function, there are, however, some differences. It is therefore possible that an alternative cofactor may be utilized for redox or structural roles in prokaryotic NOSs. BLAST searches of bacterial genome databases reveal proteins with significant identity to the C-terminal reductase domain of eukaryotic NOSs, although none of these are annotated as such [26]. Homologs of the reductase domain required for full activity in eukaryotic NOS isoforms are, for example, present in *B. subtilis* and *S. aureus* genomes. Two of the bacterial proteins homologous of the oxygenase domain of NOSs, namely deiNOS and bsNOS from *Deinococcus radiodurans* and *B. subtilis*, respectively, have recently been expressed and the recombinant protein biochemically characterized [24, 25]. The enzymes were both reported to be functional NOSs. Despite the lack of an N-terminal extension, both recombinant proteins were predominantly dimeric.

In this paper, we report the crystal structure of SANOS, a protein from methicillin-resistant *S. aureus* (MRSA), which is related to the oxygenase domains of murine iNOS and bovine eNOS. We show that the overall structure of the SANOS dimer is similar to the eukaryotic NOS oxygenase domain; however, due to the lack of an N-terminal extension in bacterial NOSs, alternative interactions promote dimer formation. The SANOS ligand binding site, equivalent to the eukaryotic H₄B binding site, contains an NAD⁺ moiety.

Results and Discussion

Overall Structure

The structure of SANOS was determined by molecular replacement with the human eNOS dimer [11] as the search model using 3.5 Å resolution X-ray data (Table 1, data set 1). The structure was refined with X-ray data to 2.4 Å (Table 1, data set 2). The current SANOS refined model contains 345 residues in each protein chain (together with one histidine from the N-terminal hexahistidine tag in the A chain and two histidine residues from the B chain), two haem groups together with two SEITU, two NAD⁺, two sucrose, and 382 water molecules, and has an overall R factor of 0.177 (R_{free} 0.241) against all data to 2.4 Å resolution. The geometry of the model is good, with rms deviations from ideality of 0.007 Å for bond lengths and 1.21° for bond angles. The three-dimensional structure of SANOS overlaps with that of

residues 133–499 of murine iNOS and residues 125–491 of bovine eNOS. There are some significant differences between bacterial and mammalian NOSs, as SANOS lacks the N-terminal extension of the eukaryotic NOSs that is required in the latter for stable dimerization [27–31]. There are also residues that are only conserved between the bacterial enzymes (Figure 1). Despite the lack of an N-terminal extension, SANOS is a dimer, and in the interface ligand binding site we see NAD⁺ present (Figure 2A). The overall topology and quaternary structure of SANOS and its relationship to the corresponding region of the previously determined N-terminal oxygenase domains of eukaryotic NOSs dimers are shown in Figures 2B–2D. The two monomers are related by approximately 2-fold symmetry (178.5°). However, the orientation of the symmetry axis is slightly different to bovine eNOS such that if the A chains are overlapped, there is a 5.3° offset between the B chains. 309 and 308 out of 350 C α s from SANOS were superimposed with an overall rms deviation of 0.78 Å and 0.93 Å for the bovine eNOS and murine iNOS monomers, respectively. The small deletions seen in the sequence alignment (Figure 1) all occur in solvent-exposed loops resulting in minor structural differences for these regions.

Haem Binding and Active Sites

The haem is buried in the interior of each monomer (Figures 2B, 2C, and 3C). The residues in the haem binding motif that contact the haem in the eukaryotic NOSs are conserved in SANOS, making extensive contacts with the side chains of Trp56, Arg51, Cys62, Pro104, Phe222, Asn223, Gly224, Trp225, Met227, Glu230, Trp316, Phe342, and Tyr344. As previously seen in the structures of mammalian NOS isoforms, there is a significant deviation from planarity of the haem [9–11].

SEITU is an inhibitor of NOSs, and is competitive with respect to arginine binding in the active site [32, 33]. SEITU binding to SANOS is similar to that observed previously in bovine and human eNOS and human iNOS (Figure 3C) [9, 11]. The nitrogens of the ureido group hydrogen bond to the conserved Glu230 side chain and one of the nitrogens also forms a hydrogen bond to the main chain carbonyl of Trp225, while the ethyl group makes van der Waals contacts with Pro203, Ile205, and Phe222. In the mammalian NOSs, Ile205 is always a valine, while in the bacteria it is generally an isoleucine, suggesting that SANOS and other bacterial NOSs may have a different selectivity and affinity for the isothioureas.

Catalytic Activity of SANOS

The conservation of residues observed in the SANOS active site suggests that the protein is an active NOS oxygenase domain. Since a prokaryotic reductase protein that interacts with SANOS remains to be characterized, NADPH and oxygen-dependent production of NO cannot be directly determined for a complete bacterial system. NOS activity has previously been measured in an assay with bacterial NOSs reconstituted with a mammalian reductase domain; however, the relevance of this to prokaryotic NOS activity is unknown [24, 25]. Nevertheless, the activity of the oxygenase domains is normally assayed directly by measuring nitrite produc-

Table 1. X-Ray Data Collection and Refinement

Data collection details	Data set 1	Data set 2
X-ray source	In house	ESRF ID14-EH2
Wavelength (Å)	1.54	0.933
Space group	<i>P</i> 2 ₁ ,2 ₁	<i>P</i> 2 ₁ ,2 ₁
Unit cell dimensions (a, b, c in Å)	65.45, 115.65, 124.07	65.78, 115.14, 126.02
Resolution range (Å)	30–3.5	30.0–2.40
Observations	26,608	169,640
Unique reflections	11,133	36,617
Completeness (%)	89.2	95.8
$\langle I/\sigma(I) \rangle$	3.3	6.8
R_{merge}^a	0.168	0.126
Outer resolution shell		
Resolution range (Å)	3.62–3.50	2.49–2.40
Unique reflections	959	3,634
Completeness (%)	77.7	96.5
$\langle I/\sigma(I) \rangle$	1.8	1.3
R_{merge}^a	0.302	0.439
Refinement statistics		
Resolution range (Å)		30.0–2.40
No. of reflections (working/test)		34,763/1,818
R factor ($R_{\text{work}}/R_{\text{free}}^b$)		0.177 (0.182/0.241)
No. of atoms (protein/water/others)		5,724/382/196
Rms bond length deviation (Å)		0.007
Rms bond angle deviation (°)		1.2
Mean B factor (Å ²) ^c		34/39/41/47
Rms backbone B factor deviation (Å ²)		4.1

$$^a R_{\text{merge}} = \sum |I - \langle I \rangle| / \sum \langle I \rangle$$

$$^b R \text{ factor} = \sum |F_o - F_c| / \sum F_o$$

^c Mean B factor for protein main chain, side chain, water, and ligand atoms, respectively.

tion from N-hydroxy-L-arginine in an H₂O₂-supported reaction [34, 35]. This reaction does not require the presence of H₄B in mammalian NOSs [34]. We observed nitrite production in SANOS with a rate of 0.15 ± 0.01 nmol nitrite produced nmol SANOS⁻¹ min⁻¹, which is within a factor of five for deiNOS activity and in common with deiNOS, much less than reported for nNOS [24].

Comparison of the Dimerization of SANOS with Mammalian NOSs

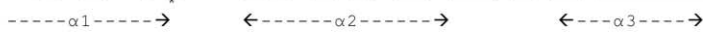
The dimerization interface of SANOS is defined by four regions (Figures 1 and 3A). Regions II and IV form the majority of the interactions in the interface. In addition to homologous subunit contacts at regions I–IV, mammalian NOSs also interact via two regions of the N terminus, namely the N-terminal hook and by two cysteines that form a tetrahedrally coordinated zinc-tetrathiolate at the dimer interface (Figure 1) [9, 11]. This region is required for dimer stability and full catalytic activity in mammalian NOS isoforms [27–31]. The importance of this region is shown by the behavior of truncated mammalian proteins. Murine iNOS Δ114 (residues 115–498) displays significant perturbation of the interface secondary structure: region IV is fully disordered, region II is partially disordered, and the α₉ helix (SANOS α₁₃; contains region III) is rotated through 35° [8]. Moreover, truncated bovine eNOS is predominantly monomeric, has only 12% of the activity of the full-length oxygenase domain, and aggregates rapidly in the absence of ligands, suggesting that it is similarly structurally unstable [29]. The absence of an N-terminal extension in SANOS (and other bacterial NOSs) compared to mammalian

NOSs and the resulting overall reduction in buried accessible surface area (2132 Å² for SANOS compared with nearly 3000 Å² in bovine eNOS) [23], does not prevent the formation of dimers for these bacterial NOSs. This implies that there could be compensatory changes in SANOS, and the other bacterial NOSs, to maintain dimer stability. We have analyzed differences in the subunit contacts between SANOS and the eukaryotic NOSs in terms of hydrogen bonding and potential hydrophobic interactions. While the contacts are largely similar, there are two differences. First, in common with the mammalian proteins, SANOS has extensive contacts between the two antiparallel α₁₂ helices (Figure 3A; residues 259–280, region II) [9–11]; in SANOS, Phe262A forms a close interaction through favorable edge-on (T-geometry) π–π interactions with Tyr273B and Tyr276B (these residues are all leucines in bovine eNOS), and it therefore seems likely that the interactions between these helices are stronger in SANOS (Figure 3A). However, since these residues are largely leucines in all other bacterial NOSs, generally the interactions between region II in the bacterial NOSs are likely to be similar to mammalian NOSs. Second, Pro323 in region IV is conserved in all bacterial NOSs while it is a glycine in all mammalian NOSs (Figure 3A). Region IV interacts with regions I, II, and IV on the opposite subunit, as well as with the interface ligand site. Pro323 might reduce the conformational flexibility and increase the hydrophobic packing, and thus strengthen the interactions of this region at the dimer interface. However, it seems unlikely that dimer stabilization of bacterial NOSs is due solely to a single residue at the subunit interface.

Turning to changes that might have a more indirect effect on the bacterial NOS dimer formation, residues

bovine eNOS 66 EGPKFPRVKNWELGSIYDTLCAQSQDGPCTPRCCLGSLVLPKRLQTRPSGPPFAEQ
human nNOS 301 KCRFRFLKVNWTEVVLTDTLHLKSTLETGCTEYICMGSIMHPSQHARRPED-VRTKGO
murine iNOS 74 TRPQYVRIKNWGSSELHDLTLLHKATSDFCTCKSKSLGSIIMNPKSLTRGPRDKPTPLEE
B subtilis 1 -----MEEKERL
B halodurans 1 -----MNQTRVRQHDGOL
B stearo 1 -----MSKTKOL
B anthracis 1 -----ML
S epidermis deiNOS 1 -----MSCPAAAVL
SANOS 1 -----M

bovine eNOS 126 LLSQARDFNQYSSIKKSGCAHEERLQEWAEVASTGTYLHRESLEVEGAKQAWRNAPR
human nNOS 360 FPPAKAEFDQYSSIKKFGKAHMRLEENKEIDTTSTYQLKDTDLIYGAKHAWRNASR
murine iNOS 134 LPHAEFENQYGSFKEAKIEHLARLEAWTKEIETTGTYYQLLDELIFAKMAWRNAPR
B subtilis 3 WNEAKAFIAACYQELGS--EBEYKDLRALTKSEIDLGTGYVHTKELHEHGAKMAWRNSNR
B halodurans 8 LQEAESFTTKCYELGS--GELSKLEERKEIDPKTGYVHTKELHAHGAKMAWRNSNR
B stearo 14 MKKAEQFTMASVRELGS--EEMRRRLNEIRWEIQTGTYYRHTYELSYGAKMAWRNSNR
B anthracis 8 IEASHFTICVYKELSEHFIE--BRMKEIQAEIEKTTGYVHTFEELVHGAKMAWRNSNR
S epidermis deiNOS 3 LDKARSFQTMSELKYN--TNEVENRKEIEQENLTCGYVHTYELSYGAKMAWRNSNR
SANOS 10 TPKMAAFRRRFEHVEE--PGLPARLRAVEEAGLWVPSAELTSGAKMAWRNSNR
3 FPEAAQAFENMKECHYE--TQIENKRLHDELEIKETGTYYHTFEELIYGAKMAWRNSNR



bovine eNOS 186 CVGRFQWGLQVFDARDCSAQEFITYICNHIKATNRGNLRSAITVFPQAPGRGDFR
human nNOS 420 CIGRFQWSKLQVFDARDCTAHGMENYICNHKATNRGNLRSAITVFPQRTDGKHDFR
murine iNOS 194 CIGRFQWNLQVFDARDCSTAQEFQHCIRHILATNNGNIRSAITVFPQSDGKHDFR
B subtilis 61 CIGRLFWSNLVDRRDVREKEDALFHIEATNNGKIRETITIFPEEKGEKQVRI
B halodurans 64 CIGRLFWSKHLVLDRCRQTEEBEAELVDHITATNDGKIETISVFRPFPNKGQVRI
B stearo 73 CIGRLFWSLYVLDAREAVVDEESYLFHIEATNNGKIRETITIFRPN---GEVRI
B anthracis 67 CIGRLFWSKMHVLDAREVNDDEEGVYHALIHIKATNDGKIVPTITIFKQYQGEENNRI
S epidermis deiNOS 62 CIGRLFWSNLVVDARDVCEKFEIKIHTHIKATNNGKIKPIYITIFSPPE---DTPKI
63 CVGRLYWELSVRDLRLINLAQAVYEAALLOHDDAFCCGHIRVVISVFGPG---VRL
SANOS 62 CIGRLFWSNLVVDARDVDEASFLSSITVYHITOATNBGKIKPIYITIVAPK---DGPKI



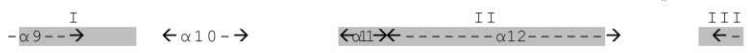
bovine eNOS 246 WNSQLIRYAGYRQDGSVIRGDPANVEITEICIQHWTPGNRFVLPPLLOA-PDEAPEL
human nNOS 480 WNSQLIRYAGYKPPDGGSTIGDPANVQFTEICIQGWKPPRGRFVLPPLLOA-NGNDPEL
murine iNOS 254 WNSQLIRYAGYMPDGTIRGDAITTEFTQICIDLGWKPRYGRFVLPPLLOA-DGQDPEV
B subtilis 121 WNHQLIRYAGYSJGDE--RIGDPASCSLTAACEELGWRGERTDFDLPLIFRMRKGDQPVW
B halodurans 124 WNHQLIRYAGYEGDQ--VIGDPISTKFTQACERLGSWERTDFVLPPLVQD-GSKPKW
B stearo 129 WNHQLIRYAGYTEEC--IGDSSSTFTTRACEQLGWKERTDFVLPPLVQW-GGQKPVW
B anthracis 123 WNHQLIRYAGYKTEMC--VIGDSSHSTAFDFCELGSWERTDFVLPPLVFS-DGKAPIY
S epidermis deiNOS 118 WNHQLIRYAGYEN---VIGDSEKVVTRAEHLGWKRGWERTDFLPLIYQ-PNDTIKI
117 HNPQLIRYADDPIN---ADFVDKRR---FGWQPRGERFVLPPLLEV-NGRAEL
SANOS 118 WNHQLIRYAGYEN---GDPAEKEVTRAEHLGWKRGWERTDFVLPPLIYQ-PNESVKF



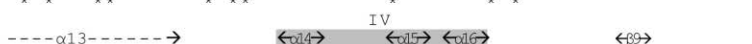
bovine eNOS 305 FVLPPELVLEVPTEHPTLEWFAALGLRWYALPANSNMLEIGGIESSAAPFSGWYMGTEI
human nNOS 539 FQLPPELVLEVPTEHPTLEWFAALGLRWYALPANSNMLEIGGIESSAAPFSGWYMGTEI
murine iNOS 313 FELPPELVLEVPTEHPTLEWFAALGLRWYALPANSNMLEVGGIESSAAPFNWYMGTEI
B subtilis 180 FELPRLSLVEVPTIHPDIEAPSLDLKWKYVPTIISMKLEVGGIHYAAPFNWYMGTEI
B halodurans 182 FAVPNEVSVKEVTEHPTLEWFAALGLRWYALPANSNMLEIGGIESSAAPFNWYMGTEI
B stearo 187 TTPKPELVLEVPTEHPTLEWFAALGLRWYALPANSNMLEIGGIESSAAPFNWYMGTEI
B anthracis 181 KEIPKEVLEVPTEHPTLEWFAALGLRWYALPANSNMLEIGGIESSAAPFNWYMGTEI
S epidermis deiNOS 172 HELPSPVLEVPTEHPTLEWFAALGLRWYALPANSNMLEIGGIESSAAPFNWYMGTEI
165 FELPPELVLEVPTEHPTLEWFAALGLRWYALPANSNMLEIGGIESSAAPFSGWYMGTEI
SANOS 172 FEYVETSLKKEVTEHPTLEWFAALGLRWYALPANSNMLEIGGIESSAAPFNWYMGTEI



bovine eNOS 365 GTRNLCDPHRYNLEEDVAVCMDDLDRTTSSLWKDKAAVEINLAVLHSEQLAKVITVDHHA
human nNOS 599 GVRDYCDNSRYNLEEVAKKWNLDMRKTTSSLWKDQALVEINLAVLYSFSQDKVITVDHHS
murine iNOS 373 GVRDFCDTQRYNLEEVERRMGLTEHTLASLWKDRAVTEINLAVLHSEFKQONVITVDHHT
B subtilis 240 GARNLADKRYNLEKLVASVGLAADYNTDLWKDQALVELNKAVALHSEKKGVSIVDHH
B halodurans 242 GARNLADEDRYNLEPKVAEYMGSLTCKDSSLWKDKALVELNVALLYSKKQBGVSIVDHH
B stearo 247 GARNFADRYNLEPKVASCMLDNTSNASLWKDKALVELNVALLYSKKAGVSIVDHH
B anthracis 231 GARNLADHDYRNLPAVAEMDDLDTSRNGLWKDKALVELNVALVHSEFKKQVSIVDHH
S epidermis deiNOS 232 AVRNLEADYRYNLEKVAEAEFEEDTKNSENKDRALVELNVALVHSEFKADGVSIVDHHT
224 AARLADYVGRYQLPAVARALGLDTSRERLWDRALVELNVALVHSEDAAGVKADHHT
SANOS 232 GVRNFDYRYNLEKVAADAFEFDTLKNSENKDRALVELNVALVHSEFKKQBGVSIVDHT



bovine eNOS 425 ATVSFEMHLDNEQKARGGCPADWAWLVPPSGSLTPVFHQEMVNYLISPAFRYQPDPEWKG
human nNOS 659 ATESFIKHMEYRRCRGGCPADWAWLVPPSGSLTPVFHQEMLYRITPSFYYQPDPEWNT
murine iNOS 433 AAESEFMHMONEYRARGGCPADWAWLVPPSGSLTPVFHQEMLYNLSPEFYQIEPWKT
B subtilis 300 AASQKFEKEEAEAGKLTGDWVLIPLPSPARTHIFHRSYDNSIVKPNFYQDKPYE-
B halodurans 302 AARQFARFEQABQAARAKVTGRWSLIPSPARTHIFHREYEDETVLPNFYQAPYES
B stearo 307 AARQFQLEFQEBKAAGRVTGDWVLIPLPSPARTHIFHRTYDNTVLPNFYQDRPYER
B anthracis 301 AAQDFQLEFQEBKAAGRVTGDWVLIPLPSPARTHIFHRTYDNTVLPNFYQDRPYER
S epidermis deiNOS 292 AAKQFEMPERNEHQQRNDVTGKWSWLAAPLSPITLSNHHGVDNTHHTNFFYKKEEPMK
284 VTAHVVRFEERARAGREVRCKKWSWLAAPLSPITLSNHHGVDNTHHTNFFYKKEEPMK
SANOS 292 AAKQFELFERNEAQQGQVTKKWSWLAAPLSPITLSNHHGVDNTHHTNFFYKKEESNA



largely common to the bacterial NOSs were mapped onto the structure of SANOS to see whether they were located in a position to influence dimerization (Figures 1 and 3B). Three of the conserved residues, Leu66, Phe67, and Gln295, line the pocket where the haem edge is exposed. This region of the protein has been suggested as an interaction site for the reductase domain; the conservation of these residues between bacterial species is consistent with this hypothesis [24]. Mapping of the electrostatic potential of the solvent-accessible surfaces of SANOS and a comparison with the mammalian NOSs (data not shown) indicates a weak but not striking conservation of positive charge in this region. Further biochemical and structural data are needed to define the putative SANOS interface with the reductase protein. Seventy-eight percent of the conserved residues cluster between the protein core and the dimer interface. In addition to van der Waals interactions, a number of hydrogen bonds are found: Glu16, Gln295 (through a water molecule), and Arg308 hydrogen bond to the universally conserved Arg57, Trp225, and Glu303, respectively; in addition, bonds between Glu300 and Tyr333, and Thr311 and Asn60 are also seen. In the case of deiNOS, there are some changes from otherwise conserved residues in other bacterial species (Figure 1), but it seems likely that the substituted residues (Gln295 to His, Thr311 to Arg, and Asn60 to Thr) will also form hydrogen bonds in a similar manner. Many of the interactions formed in SANOS by the residues conserved in bacteria in SANOS are in the vicinity of helix α 13, suggesting that the movement of this helix seen in the iNOS Δ 114 structure will not occur. One explanation for the instability of truncated mammalian NOSs may be that the N-terminal extension also makes intrachain interactions with residues in the region of helices α 13 and α 16 that may stabilize the secondary structure of the monomeric interface elements, thus allowing dimerization to occur. In the absence of the N-terminal extension, the monomeric interface structure is destabilized, pushing the monomer/dimer equilibrium toward monomer and/or aggregation. It is possible for SANOS that the conserved residues stabilize the monomeric tertiary structure relative to the truncated mammalian proteins, thereby allowing dimer formation and thus compensating for the absence of the N-terminal hook.

Subunit Interface Ligand Site

The subunit interface ligand site in the mammalian NOS binds H₄B. H₄B appears to have a dual role: it both stabilizes the dimer and participates in catalysis [7, 23]. While SANOS shares the overall topology of the interface ligand binding site with the mammalian NOSs, there are, however, some key differences [9–11]. Many of the residues that mediate NOS-H₄B binding through hydrogen bonding and van der Waals interactions are largely

conserved, suggesting that this region has a functional role in SANOS [9–11]. However, the binding site is more open to the solvent, due to the absence of the N-terminal extension. In the mammalian NOSs, 2 residues from this region, for example, bovine eNOS Ser104 and Val106, interact with the C6 and N5 atoms of H₄B, respectively, giving rise to the stereospecificity of the NOS-H₄B interaction [9, 23]. Since these residues are not present in SANOS and as it is thought that H₄B is not present in prokaryotes, it is possible that an alternative cofactor will bind at this site. The increased volume of this ligand site in the prokaryotic NOSs could imply that a larger molecule can be accommodated than for mammalian NOSs. Density for the nicotinamide, ribose, and the pyrophosphate group of NAD⁺ (which was used as an additive to improve crystallization) can be seen in the interface ligand binding site of the SANOS structure (Figure 2A); however, density is not observed for the adenosine moiety of NAD⁺. The nicotinamide ring of NAD⁺ stacks between the side chains of Trp316A and Tyr329B, while the amide nitrogen hydrogen bonds to the haem propionate. In bovine eNOS, the pterin of H₄B is similarly sandwiched between the structurally homologous Trp449A and Phe462B while the haem propionate hydrogen bonds with the pyrimadone moiety of the pterin (Figure 3C) [9]. The pyrophosphate group is in the space occupied by residues 103–104 of bovine eNOS (in the N-terminal extension; Figure 3C) and are stabilized by hydrogen bonds with the side chains of Lys318 and Ser313 [9]. Since NAD⁺ is involved in redox reactions in the cell, its presence at the site may be functionally significant, although the involvement of nicotinamide adenine dinucleotide in bacterial NOS function has not been reported. Experiments to investigate whether NAD⁺ or other redox cofactors present in prokaryotes are able to stimulate nitrite production were carried out using the hydrogen peroxide shunt assays with H₂O₂-supported N-hydroxy-L-arginine oxidation (Table 2). In contrast to the mammalian NOSs, where addition of the cognate interface ligand causes a 2- to 3-fold increase in activity, in common with deiNOS, H₄B has no stimulatory effect on the activity of SANOS, which may suggest a different cofactor is required for full enzyme activity [24, 34, 36]. Further experiments showed there was no stimulation over basal levels of activity for NAD⁺, NADH, and β -nicotinamidemonucleotide. It is possible that the observed NAD⁺ binding to SANOS might be an example of molecular mimicry such as has been previously seen in mammalian NOSs where arginine binding at the interface site has previously been reported for bovine eNOS [9]. Given the disordering of the adenosine portion of NAD⁺, a further possibility to consider is whether the presence of the cognate bacterial reductase protein might be required to correctly position NAD⁺ and thereby allow a role in catalysis.

Figure 1. Sequence Alignment of SANOS with Eukaryotic and Prokaryotic NOSs

The alignment was carried out using ClustalW and colored using Boxshade. Filled residues indicate amino acid identity and shaded residues indicate similarity [40]. SANOS secondary structure and the regions involved in the dimerization interface (233–240 [I], 259–280 [II], 288–291 [III], and 314–330 [IV]) are indicated below the alignment. Key residues are indicated as follows: †, cysteines forming zinc tetrathiolate in mammalian NOSs (above the alignment); *, residues that are largely conserved in bacteria (below the alignment). The complete N-terminal sequence for the *B. subtilis* NOS is not shown, as it is not clearly assigned.

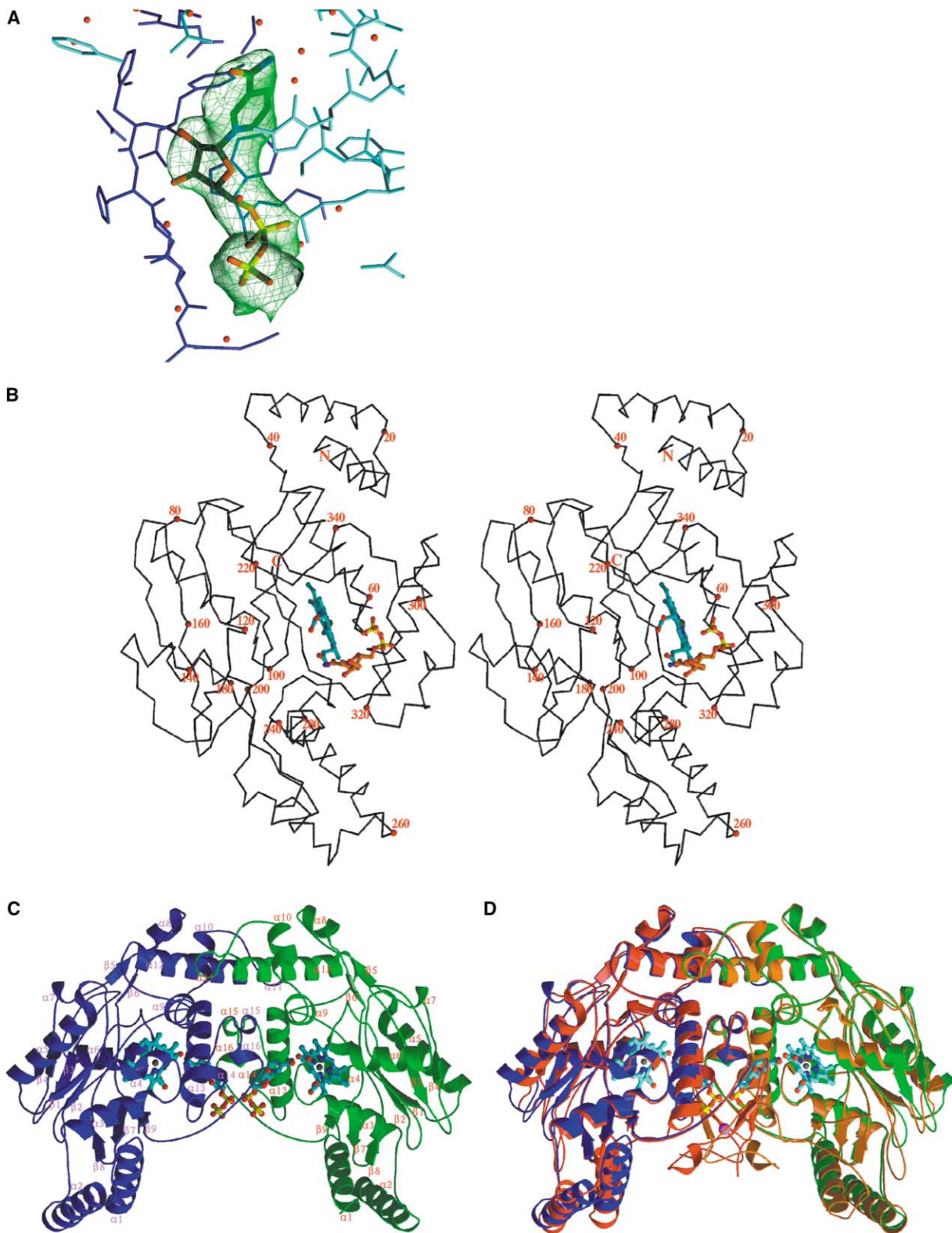


Figure 2. The Topology and NAD⁺ Binding of SANOS

(A) $|F_o| - |F_c|$ 2.4 Å simulated annealing omit electron density map showing the nicotinamide, ribose, and pyrophosphate of NAD⁺ bound at the interface ligand binding site; electron density for the adenosine moiety is absent. The A chain is colored blue and the B chain is colored cyan. The small red spheres represent water molecules.

(B) Stereo diagram of the SANOS monomer C_α backbone. The N and C termini and every twentieth residue are indicated in red. The NAD⁺ and haem are shown as a ball-and-stick models with the iron of the latter indicated by a gray sphere.

Other candidate redox active molecules that we have considered include the eubacterial pterin molybdopterin dinucleotide, although attempts to model this into SANOS resulted in steric clashes, suggesting that this is not the biological cofactor (data not shown). It has been reported that both tetrahydrofolate (THF) and H₄B supported the oxygenase activity of *D. radiodurans* and *B. subtilis* NOSs, when reconstituted in an artificial system with a mammalian nNOS reductase domain [24, 25]. The fact that H₄B (which is thought not to be present in bacteria) can stimulate this hybrid species reconstitution assay also brings in to question the relevance of such results. However, THF can be modeled into the interface ligand site of SANOS, consistent with the hypothesis that it, or a related pterin, may be the biological ligand (data not shown). Importantly, THF fails to stimulate the rate of reaction in the SANOS shunt assay (Table 2). Clearly further work is required to identify the nature of the intersubunit ligand, if any. In particular it will be necessary to set up assay systems with SANOS and the cognate bacterial reductase protein to be able to unequivocally define this cofactor.

Biological Implications

The discovery of bacterial enzymes that are homologous to the eukaryotic NOSs oxygenase domain means that the biological role of NO in prokaryotes needs to be reexamined. NO may be a novel bacterial signaling molecule and may be important to host-pathogen interactions, possibly by activation of either generalized or specific responses in the host or bacteria.

We report here the X-ray crystal structure of a functional nonmammalian NOS oxygenase domain, SANOS, from MRSA, which shows an overall topology related to the eukaryotic NOS oxygenase domain. However, despite the lack of an N-terminal extension necessary for stable dimerization of the eukaryotic NOSs, SANOS is a dimer. A comparison with eukaryotic NOSs suggests that while there are some differences in subunit interface interactions for SANOS, it is likely that dimerization of the bacterial NOSs are a function of the conserved residues in the prokaryote enzymes that stabilize the tertiary structure of the monomer. The ligand binding sites, with the exception of the interface site, are analogous to the mammalian NOSs. The interface ligand site of SANOS is more open; this may reflect the fact that in contrast to the bifunctional mammalian NOSs, SANOS has to interact with a separate reductase protein. Alternatively, the larger volume of the pocket might reflect a requirement to accommodate a bulkier ligand such as the NAD⁺ seen bound in this structure or possibly THF [24, 25]. However, the physiological ligand remains to be identified. The determination of the structure of SANOS, together with a comparison with eukaryotic NOSs, gives an important insight into the structure/function relation-

ships of such NOSs and provides a focus for further investigations into the biochemistry and biological role of prokaryotic NOSs.

Experimental Procedures

Cloning, Expression, and Purification of Recombinant SANOS from *S. aureus*

PCR using *Pfu* DNA polymerase (Stratagene) was used to amplify the coding region from amino acid 2 using MRSA genomic DNA as a template (the MRSA genomic DNA was a gift from Dr. Michael Lockyer; Arrow Therapeutics, London, UK). A pair of primers was synthesized (Genosys) for PCR experiments. The sequences of the primers were: 5' primer: 5'-CGCATATGGGAGGACACCACCACCAC CACCCTTATTTAAAGAGGCTCAAGCTTTCATAGAAACATG-3' and 3' primer: 5'-CGTCTAGATTAATGATGGAAAGGGCACTGG-3'. A hexahistidine coding sequence motif is designed into the 5' primer to facilitate purification of the recombinant protein by metal affinity chromatography. The oligonucleotides also incorporate NdeI and XbaI sites into the 5' and 3' primers, respectively, in order to facilitate cloning. The *sanos* fragment was cloned into the vector pCWORI, and DNA sequence analysis of the cloned product showed that the sequence was identical to that deposited in the sequence database. The resulting plasmid was transformed into *E. coli* BL21 (DE3) (Novagen) for protein expression.

BL21 (DE3) harboring the *sanos* expression plasmid were grown in a 200 ml luria broth starter culture supplemented with 100 $\mu\text{g ml}^{-1}$ ampicillin at 30°C for 8 hr. Five milliliter aliquots of this culture were used to inoculate 18 \times 500 ml cultures of Terrific broth supplemented with 100 $\mu\text{g ml}^{-1}$ ampicillin, which were grown at 23°C for 10 hr. IPTG and γ -aminolevulinic acid were then added to 250 $\mu\text{g ml}^{-1}$ and 100 $\mu\text{g ml}^{-1}$, respectively, and induction was carried out at 23°C for 48 hr. The cell pellet was recovered by centrifugation at 6000 \times g for 6 min at 4°C. Approximately 40 g of *E. coli* cells was sonicated in a final volume of 1 L 50 mM K phosphate (pH 7.2), 150 mM NaCl, 1 mM DTT (buffer 1). The sonicated cell suspension was clarified by centrifugation at 2,500 \times g for 42 min at 4°C and the supernatant was loaded onto a 130 ml chelating Sepharose column (Amersham Biosciences) that had been charged to one-third capacity with zinc sulfate and equilibrated in buffer 1. The column was then washed with 500 ml of buffer 1 and then eluted with a 1 L 0–0.1 M imidazole gradient in buffer 1, and 10 ml fractions were collected. The fractions were analyzed by SDS-PAGE and those containing pure SANOS were pooled. This purification protocol produced on average 40 mg pure SANOS. Two milligram aliquots were stored at –80°C.

Assays of H₂O₂-Supported N-Hydroxy-L-Arginine (NOHA) Oxidation

H₂O₂-dependent NOHA oxidation was assayed at 37°C. One milliliter assays were set up containing 150 nM SANOS and 10 u superoxide dismutase in 50 mM HEPES (pH 7.5), 0.5 mM DTT. Reactions without enzyme were used as a blank. All reactions were preincubated at 25°C for 30 min and were initiated at 37°C by addition of 50 μl of 10 mM NOHA and 3.4 μl of 30% H₂O₂. Two 250 μl aliquots were taken at 3 min and stopped by addition of 250 μl of Griess reagent to each tube; a further two aliquots were taken and stopped after 60 min. The absorbance at 540 nm was used as a measure of nitrite production. All reactions were carried out in triplicate. The effect of ligands was examined by addition of 0.1 mM ligand to the reaction mixture. The program Origin (Microcal) was used to calculate reaction rates.

Crystallization

SANOS was defrosted in the presence of 2 mM L-arginine (Sigma) and concentrated to 10 mg/ml using a Centricon 10 (Millipore) at

(C) Ribbon diagram of the SANOS dimer. The subunits are colored blue and green. The haems and the interface NAD⁺s are shown as ball-and-stick models with the haem iron represented by a gray sphere. The secondary structure elements are labeled for both A and B chains. (D) Ribbon diagram of the overlapped SANOS and bovine eNOS dimers. The subunits are colored blue and green for SANOS, and red and orange for bovine eNOS. The haems and the interface NAD⁺s from SANOS are shown as ball-and-stick models, with the haem iron represented by a gray sphere. The interface zinc in bovine eNOS is shown as a large magenta sphere.

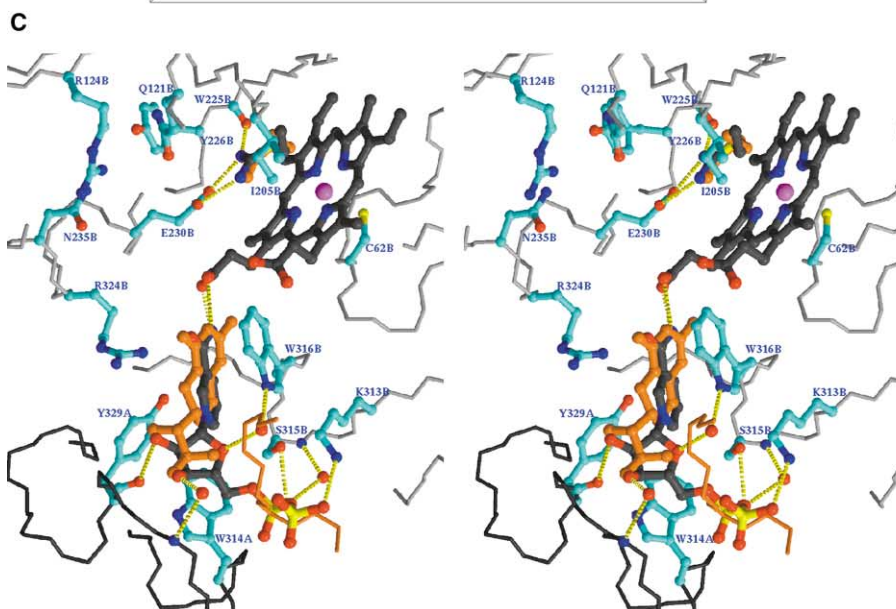
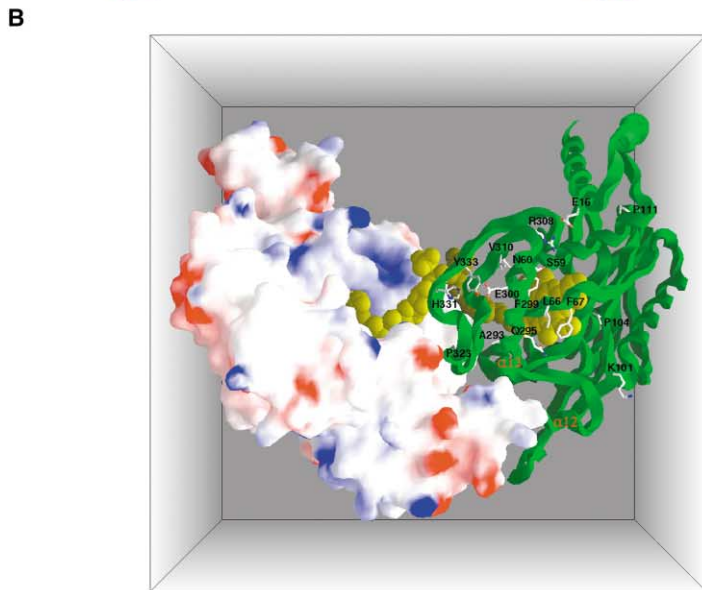
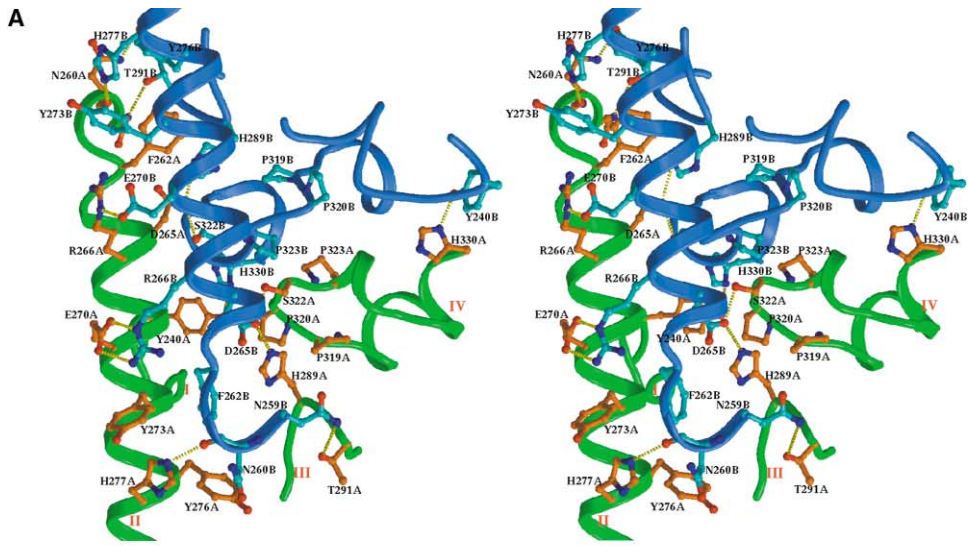


Table 2. Assays of H₂O₂-Supported N-Hydroxy-L-Arginine (NOHA) Oxidation

Ligand ^a	Reaction rate (nmol nitrite produced nmol SANOS ⁻¹ min ⁻¹)	Fold stimulation of activity over unliganded enzyme
None	0.15 ± 0.01	—
H ₂ B	0.16 ± 0.01	1.09 ± 0.09
NAD ⁺	0.15 ± 0.01	1.03 ± 0.10
NADH ₂	0.17 ± 0.05	1.12 ± 0.33
β-Nicotinamidemononucleotide	0.19 ± 0.03	1.24 ± 0.19
Tetrahydrofolate	0.17 ± 0.01	1.14 ± 0.07

^a100 μM of ligand used.

18°C. Gel filtration was performed at 21°C in the absence of ligands using a Superose 12 HR10/30 column (Amersham Biosciences) to remove aggregated protein. The column was equilibrated with crystallization buffer (25 mM Tris [pH 7.4], 50 mM NaCl, 1 mM DTT). The peak fractions were pooled and concentrated to 10 mg/ml as described above and used immediately for crystallization.

Crystals were obtained by the sitting drop vapor diffusion method at 21°C using freshly gel-filtered and concentrated protein. S-ethylisothiourrea (SEITU; Sigma) and nondetergent sulphobetaine 195 (NDSB195; Hampton Research) were added to a final concentration of 5 mM and 0.3 M, respectively, to SANOS, giving a protein concentration of 8 mg/ml. γ-butyrolactone to a final concentration of 1%–2% was added directly to the crystallization droplets. Crystals were typically obtained from 100 mM Tris (pH 7.4), 3%–9% PEG 6000, 5% MPD. The crystals used for the high-resolution structural determination grew from a droplet that contained a further additive, 10 mM NAD⁺.

X-Ray Data Collection, Structure Determination, and Refinement

Initial X-ray data (Table 1, data set 1) were collected using an in-house system consisting of a Rigaku generator equipped with Osmic multilayer optics and a MAR 345 image plate. Higher resolution data (Table 1, data set 2) were collected at a synchrotron source (ESRF, Grenoble, France) on beamline ID14-EH2 equipped with an ADSC-q4 CCD detector. Crystals were flash-frozen for data collection in 100 mM Tris (pH 7.4), 10% PEG 6000, with 15% sucrose and 15% trehalose as cryoprotectant. The X-ray data were processed with DENZO and SCALEPACK [37]. Crystals belong to the orthorhombic space group P2₁2₁2₁, with unit cell dimensions: a = 65.8, b = 115.1, c = 126.0 Å and a dimer in the asymmetric unit.

Molecular replacement was used for the structure determination using the human eNOS dimer, deleting all residues up to residue 122 in each chain (3nos) [11], as an initial model. CNS [38] was used for molecular replacement and structural refinement.

Acknowledgments

We would like to acknowledge the staff at ESRF, Grenoble, France for help with data collection. We also thank the following: Dr. R.

Esnouf and Ms. J. Dong for computer support, Dr. K. Harlos for help with the in-house data collection, Mr. C.E. Nichols for discussions on cryoprotectants, and Dr. P. Lowe and Dr. W. Alderton for helpful discussions. The financial support of the MRC (D.K.S.), the BBSRC, and the Wellcome Trust (A.R.H.) is acknowledged.

Received: July 17, 2002

Revised: September 24, 2002

Accepted: September 30, 2002

References

- Knowles, R.G., and Moncada, S. (1994). Nitric oxide synthases in mammals. *Biochem. J.* 298, 249–258.
- Cooper, C.E. (1999). Biochemistry of nitric oxide. *Biochim. Biophys. Acta* 1411, 215–216.
- Charles, I.G., Chubb, A., Gill, R., Clare, J., Lowe, P.N., Holmes, L.S., Page, M., Keeling, J.G., Moncada, S., and Riveros-Moreno, V. (1993). Cloning and expression of a rat neuronal nitric oxide synthase coding sequence in a baculovirus/insect cell system. *Biochem. Biophys. Res. Commun.* 196, 1481–1489.
- Sheta, E.A., McMillan, K., and Masters, B.S. (1994). Evidence for a bidomain structure of constitutive cerebellar nitric oxide synthase. *J. Biol. Chem.* 269, 15147–15153.
- Brenman, J.E., Chao, D.S., Gee, S.H., McGee, A.W., Craven, S.E., Santillano, D.R., Wu, Z., Huang, F., Xia, H., Peters, M.F., et al. (1996). Interaction of nitric oxide synthase with the post-synaptic density protein PSD-95 and α1-syntrophin mediated by PDZ domains. *Cell* 84, 757–767.
- Ponting, C.P. (1997). Evidence for PDZ domains in bacteria, yeast, and plants. *Protein Sci.* 6, 464–468.
- Alderton, W.K., Cooper, C.E., and Knowles, R.G. (2001). Nitric oxide synthases: structure, function and inhibition. *Biochem. J.* 357, 593–615.
- Crane, B.R., Arvai, A.S., Gachhui, R., Wu, C., Ghosh, D.K., Getzoff, E.D., Stuehr, D.J., and Tainer, J.A. (1997). The structure of nitric oxide synthase oxygenase domain and inhibitor complexes. *Science* 278, 425–431.
- Raman, C.S., Li, H., Martasek, P., Kral, V., Masters, B.S., and Poulos, T.L. (1998). Crystal structure of constitutive endothelial

Figure 3. Detailed Structural Analysis of SANOS

(A) Stereo diagram showing the dimer interface of SANOS. The main chains are shown as ribbons and coils, with the A chain colored green and the B chain colored blue. The side chains of key residues involved in the interface interactions are shown as balls and sticks and colored orange and cyan for the A and B chains, respectively. The yellow dashed lines represent the hydrogen bonds between the two chains. The four segments from each chain are labeled I–IV (residues 233–240, 259–280, 288–291, and 314–330, respectively).

(B) Electrostatic surface (A chain) and ribbons (B chain) showing the charge distribution on the molecular surface and the dimer interface. The positively and negatively charged areas are colored blue and red, respectively. All ligands for both monomers are shown as dark yellow-colored space-filling representations. The side chains that are only conserved among bacterial NOSs are shown as balls and sticks, with the nitrogen and oxygen atoms colored in blue and red, respectively.

(C) Stereo view of one set of ligand binding sites of SANOS. The main chain backbone of the A and B chains are colored dark and light gray, respectively. Haem, SEITU, and the nicotinamide and ribose moieties of NAD⁺ are colored by atoms, with carbon atoms in dark gray. The haem iron is shown as a magenta sphere. The side chains of key residues are drawn as ball-and-stick representations and colored by atoms, with their carbon atoms in cyan. Water molecules are represented as red spheres. The broken yellow lines indicate hydrogen bonds between the substrates and the protein. SEITU, H₂B, and a section of the hook from bovine eNOS that interacts with the pterin (colored orange) have been overlaid onto the SANOS interface ligand binding site.

- nitric oxide synthase: a paradigm for pterin function involving a novel metal center. *Cell* 95, 939–950.
10. Crane, B.R., Arvai, A.S., Ghosh, D.K., Wu, C., Getzoff, E.D., Stuehr, D.J., and Tainer, J.A. (1998). Structure of nitric oxide synthase oxygenase dimer with pterin and substrate. *Science* 279, 2121–2126.
 11. Fischmann, T.O., Hruza, A., Niu, X.D., Fossetta, J.D., Lunn, C.A., Dolphin, E., Prongay, A.J., Reichert, P., Lundell, D.J., Narula, S.K., et al. (1999). Structural characterization of nitric oxide synthase isoforms reveals striking active-site conservation. *Nat. Struct. Biol.* 6, 233–242.
 12. Li, H., Raman, C.S., Glaser, C.B., Blasko, E., Young, T.A., Parkinson, J.F., Whitlow, M., and Poulos, T.L. (1999). Crystal structures of zinc-free and -bound heme domain of human inducible nitric oxide synthase. Implications for dimer stability and comparison with endothelial nitric-oxide synthase. *J. Biol. Chem.* 274, 21276–21284.
 13. Zhang, J., Martasek, P., Paschke, R., Shea, T., Siler Masters, B.S., and Kim, J.J. (2001). Crystal structure of the FAD/NADPH-binding domain of rat neuronal nitric-oxide synthase. Comparisons with NADPH-cytochrome P450 oxidoreductase. *J. Biol. Chem.* 276, 37506–37513.
 14. Wang, M., Roberts, D.L., Paschke, R., Shea, T.M., Masters, B.S., and Kim, J.J. (1997). Three-dimensional structure of NADPH-cytochrome P450 reductase: prototype for FMN- and FAD-containing enzymes. *Proc. Natl. Acad. Sci. USA* 94, 8411–8416.
 15. Cutruzzola, F. (1999). Bacterial nitric oxide synthesis. *Biochim. Biophys. Acta* 1411, 231–249.
 16. Goretski, J., Zafiriou, O.C., and Hollocher, T.C. (1990). Steady-state nitric oxide concentrations during denitrification. *J. Biol. Chem.* 265, 11535–11538.
 17. Nunoshiba, T., DeRojas-Walker, T., Tannenbaum, S.R., and Demple, B. (1995). Roles of nitric oxide in inducible resistance of *Escherichia coli* to activated murine macrophages. *Infect. Immun.* 63, 794–798.
 18. Poole, R.K., Anjum, M.F., Membrillo-Hernandez, J., Kim, S.O., Hughes, M.N., and Stewart, V. (1996). Nitric oxide, nitrite, and Fnr regulation of hmp (flavo-hemoglobin) gene expression in *Escherichia coli* K-12. *J. Bacteriol.* 178, 5487–5492.
 19. Chen, Y., and Rosazza, J.P. (1994). A bacterial nitric oxide synthase from a *Nocardia* species. *Biochem. Biophys. Res. Commun.* 203, 1251–1258.
 20. Chen, Y., and Rosazza, J.P. (1995). Purification and characterization of nitric oxide synthase (NOS_{Noc}) from a *Nocardia* species. *J. Bacteriol.* 177, 5122–5128.
 21. Choi, W.S., Chang, M.S., Han, J.W., Hong, S.Y., and Lee, H.W. (1997). Identification of nitric oxide synthase in *Staphylococcus aureus*. *Biochem. Biophys. Res. Commun.* 237, 554–558.
 22. Choi, W.S., Seo, D.W., Chang, M.S., Han, J.W., Hong, S.Y., Paik, W.K., and Lee, H.W. (1998). Methyl esters of L-arginine and N-nitro-L-arginine induce nitric oxide synthase in *Staphylococcus aureus*. *Biochem. Biophys. Res. Commun.* 246, 431–435.
 23. Raman, C.S., Martasek, P., and Masters, B.S.S. (2000). Structural themes determining function in nitric oxide synthases. In *The Porphyrin Handbook*, K.M. Kadish, K.M. Smith, and R. Guilard, eds., Volume 4 (London: Academic Press).
 24. Adak, S., Bilwes, A.M., Panda, K., Hosfield, D., Aulak, K.S., McDonald, J.F., Tainer, J.A., Getzoff, E.D., Crane, B.R., and Stuehr, D.J. (2002). Cloning, expression, and characterization of a nitric oxide synthase protein from *Deinococcus radiodurans*. *Proc. Natl. Acad. Sci. USA* 99, 107–112.
 25. Adak, S., Aulak, K.S., and Stuehr, D.J. (2002). Direct evidence for nitric oxide production by a nitric oxide synthase-like protein from *Bacillus subtilis*. *J. Biol. Chem.* 277, 16167–16171.
 26. Altschul, S.F., Gish, W., Miller, W., Myers, E.W., and Lipman, D.J. (1990). Basic local alignment search tool. *J. Mol. Biol.* 215, 403–410.
 27. Chen, P.F., Tsai, A.L., and Wu, K.K. (1995). Cysteine 99 of endothelial nitric oxide synthase (NOS-III) is critical for tetrahydrobiopterin-dependent NOS-III stability and activity. *Biochem. Biophys. Res. Commun.* 215, 1119–1129.
 28. Ghosh, D.K., Wu, C., Pitters, E., Moloney, M., Werner, E.R., Mayer, B., and Stuehr, D.J. (1997). Characterization of the inducible nitric oxide synthase oxygenase domain identifies a 49 amino acid segment required for subunit dimerization and tetrahydrobiopterin interaction. *Biochemistry* 36, 10609–10619.
 29. Rodriguez-Crespo, I., Moenne-Loccoz, P., Loehr, T.M., and Ortiz de Montellano, P.R. (1997). Endothelial nitric oxide synthase: modulations of the distal heme site produced by progressive N-terminal deletions. *Biochemistry* 36, 8530–8538.
 30. Martasek, P., Miller, R.T., Liu, Q., Roman, L.J., Salerno, J.C., Migita, C.T., Raman, C.S., Gross, S.S., Ikeda-Saito, M., and Masters, B.S. (1998). The C331A mutant of neuronal nitric-oxide synthase is defective in arginine binding. *J. Biol. Chem.* 273, 34799–34805.
 31. Ghosh, D.K., Crane, B.R., Ghosh, S., Wolan, D., Gachhui, R., Crooks, C., Presta, A., Tainer, J.A., Getzoff, E.D., and Stuehr, D.J. (1999). Inducible nitric oxide synthase: role of the N-terminal β -hairpin hook and pterin-binding segment in dimerization and tetrahydrobiopterin interaction. *EMBO J.* 18, 6260–6270.
 32. Garvey, E.P., Oplinger, J.A., Tanoury, G.J., Sherman, P.A., Fowler, M., Marshall, S., Harmon, M.F., Paith, J.E., and Furfine, E.S. (1994). Potent and selective inhibition of human nitric oxide synthases. Inhibition by non-amino acid isothioureas. *J. Biol. Chem.* 269, 26669–26676.
 33. Southan, G.J., Szabo, C., and Thiemermann, C. (1995). Isothioureas: potent inhibitors of nitric oxide synthases with variable isoform selectivity. *Br. J. Pharmacol.* 114, 510–516.
 34. Pufahl, R.A., Wishnok, J.S., and Marletta, M.A. (1995). Hydrogen peroxide-supported oxidation of NG-hydroxy-L-arginine by nitric oxide synthase. *Biochemistry* 34, 1930–1941.
 35. Ghosh, S., Wolan, D., Adak, S., Crane, B.R., Kwon, N.S., Tainer, J.A., Getzoff, E.D., and Stuehr, D.J. (1999). Mutational analysis of the tetrahydrobiopterin-binding site in inducible nitric-oxide synthase. *J. Biol. Chem.* 274, 24100–24112.
 36. Adak, S., Wang, Q., and Stuehr, D.J. (2000). Arginine conversion to nitroxide by tetrahydrobiopterin-free neuronal nitric-oxide synthase. Implications for mechanism. *J. Biol. Chem.* 275, 33554–33561.
 37. Otwinowski, Z., and Minor, W. (1996). Processing of X-ray diffraction data collected in the oscillation mode. In *Methods in Enzymology*, C.W. Carter and R.M. Sweet, eds. (London: Academic Press), pp. 307–326.
 38. Brunger, A.T., Adams, P.D., Clore, G.M., Delano, W.L., Gros, P., Grosse, K.R.W., Jiang, J.S., Kuszewski, J., Nilges, M., Pannu, N.S., et al. (1998). Crystallography and NMR system: a new software suite for macromolecular structure determination. *Acta Crystallogr. D* 54, 905–921.
 39. Pant, K., Bilwes, A.M., Adak, S., Stuehr, D.J., and Crane, B.R. (2002). Structure of a nitric oxide synthase heme protein from *Bacillus subtilis*. *Biochemistry* 41, 11071–11079.
 40. Thompson, J.D., Higgins, D.G., and Gibson, T.J. (1994). CLUSTAL W: improving the sensitivity of progressive multiple sequence alignment through sequence weighting, position-specific gap penalties and weight matrix choice. *Nucleic Acids Res.* 22, 4673–4680.

Accession Numbers

The coordinates and structure factors for the SANOS structure have been deposited in the Protein Data Bank under ID code 1MJT.

Note Added in Proof

During the review process for this manuscript, a paper was published reporting the structures of a bacterial NOS oxygenase protein from *Bacillus subtilis* complexed with arginine or N-hydroxyarginine and tetrahydrofolate in the substrate and interface ligand sites, respectively [39]. Although binding of the pterin of THF is seen in the interface ligand site, the density for the glutamyl p-aminobenzoic acid moiety is weak. Modeling of the pterin side chain results in both glutamate moieties close to one another in a negatively charged region of the protein surface. The authors therefore suggest that either the mode of binding of the pterin side chain is different to mammalian NOSs (perhaps involving another protein) or that the cognate ligand is a different cofactor.